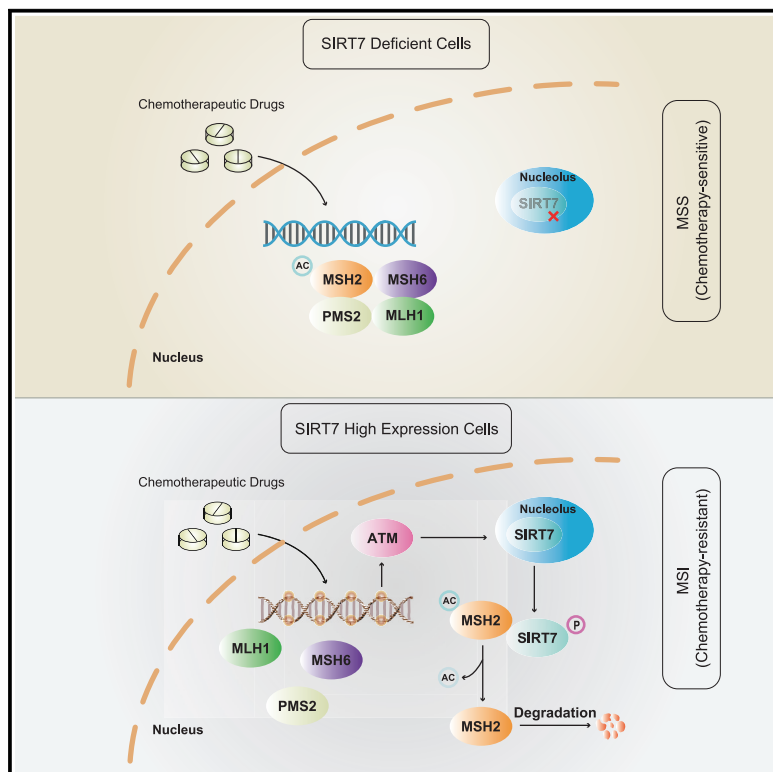


## Phosphorylation of SIRT7 by ATM causes DNA mismatch repair downregulation and adaptive mutability during chemotherapy

### Graphical abstract



### Authors

Lianhui Sun, Guangjian Fan,  
Zhuqing Zhang, ..., Baokun He,  
Shengping Zhang, Chuangui Wang

### Correspondence

spzhang@sdut.edu.cn (S.Z.),  
cgwang24@sdut.edu.cn (C.W.)

### In brief

Sun et al. identified that ATM-dependent SIRT7 phosphorylation serves as a driving mechanism for MMR impairment and MSI following chemotherapy, including 6-TG, 6-MP, and etoposide. Thus, SIRT7 phosphorylation exhibits potential as a prognostic marker for chemotherapy efficacy and a prospective target to improve the effectiveness of chemotherapy.

### Highlights

- SIRT7 triggers microsatellite instability occurrence under DNA-damaging drug treatment
- DNA-damaging drugs cause ATM kinase-dependent SIRT7 phosphorylation and redistribution
- SIRT7 phosphorylation may serve as a predictive biomarker for chemotherapeutic efficacy



## Article

# Phosphorylation of SIRT7 by ATM causes DNA mismatch repair downregulation and adaptive mutability during chemotherapy

Lianhui Sun,<sup>1,5</sup> Guangjian Fan,<sup>1,5</sup> Zhuqing Zhang,<sup>1,5</sup> Dong Chang,<sup>1</sup> Xiaoyu Zhang,<sup>1</sup> Tongqing Zhang,<sup>1</sup> Jichuan Geng,<sup>1</sup> Xiaoxia Zhang,<sup>1</sup> Menghan Lin,<sup>1</sup> Chen Hu,<sup>1</sup> Jiaqi Zhou,<sup>1</sup> Mengxue Wang,<sup>1</sup> Liu Cao,<sup>2</sup> Mary Zhang,<sup>3</sup> Baokun He,<sup>4</sup> Shengping Zhang,<sup>1,\*</sup> and Chuangui Wang<sup>1,6,\*</sup>

<sup>1</sup>Biomedical Translational Research Institute, School of Life Sciences and Medicine, Shandong University of Technology, Zibo 255049, China

<sup>2</sup>Health Sciences Institute, College of Basic Medical Sciences, China Medical University, Shenyang 110122, China

<sup>3</sup>Department of Oncology, Karmanos Cancer Institute, Wayne State University School of Medicine, 4100 John R., Detroit, MI 48201, USA

<sup>4</sup>Institute of Chinese Materia Medica, The Fourth Clinical Medical College, Guangzhou University of Chinese Medicine, Shenzhen, Guangdong 518033, China

<sup>5</sup>These authors contributed equally

<sup>6</sup>Lead contact

\*Correspondence: spzhang@sdut.edu.cn (S.Z.), cgwang24@sdut.edu.cn (C.W.)

<https://doi.org/10.1016/j.celrep.2025.115269>

## SUMMARY

Drug resistance significantly limits the efficacy of chemotherapy. The DNA mismatch repair (MMR) system maintains genomic stability by correcting DNA errors. During DNA-damaging treatments, cancer cells transiently increase their adaptive mutability, also known as microsatellite instability (MSI), to evade therapeutic pressure through MMR downregulation, conferring drug resistance. However, an understanding of the underlying mechanisms of MMR protein downregulation under DNA-damaging drugs remains limited. Our study reveals a negative correlation between SIRT7 protein levels and MMR core protein MSH2 levels in cervical and lung cancer tissues. SIRT7 destabilizes MSH2, promoting MSI and mutagenesis. Molecularly, DNA damage triggers ATM kinase-dependent phosphorylation and subcellular redistribution of SIRT7. Phosphorylated SIRT7 interacts with and deacetylates MSH2, impairing MMR, and inducing MSI and drug resistance. Our findings suggest that SIRT7 drives MMR downregulation under therapeutic stress and that ATM-dependent phosphorylation of SIRT7 may serve as a predictive biomarker for chemotherapeutic efficacy and a target for cancer treatment.

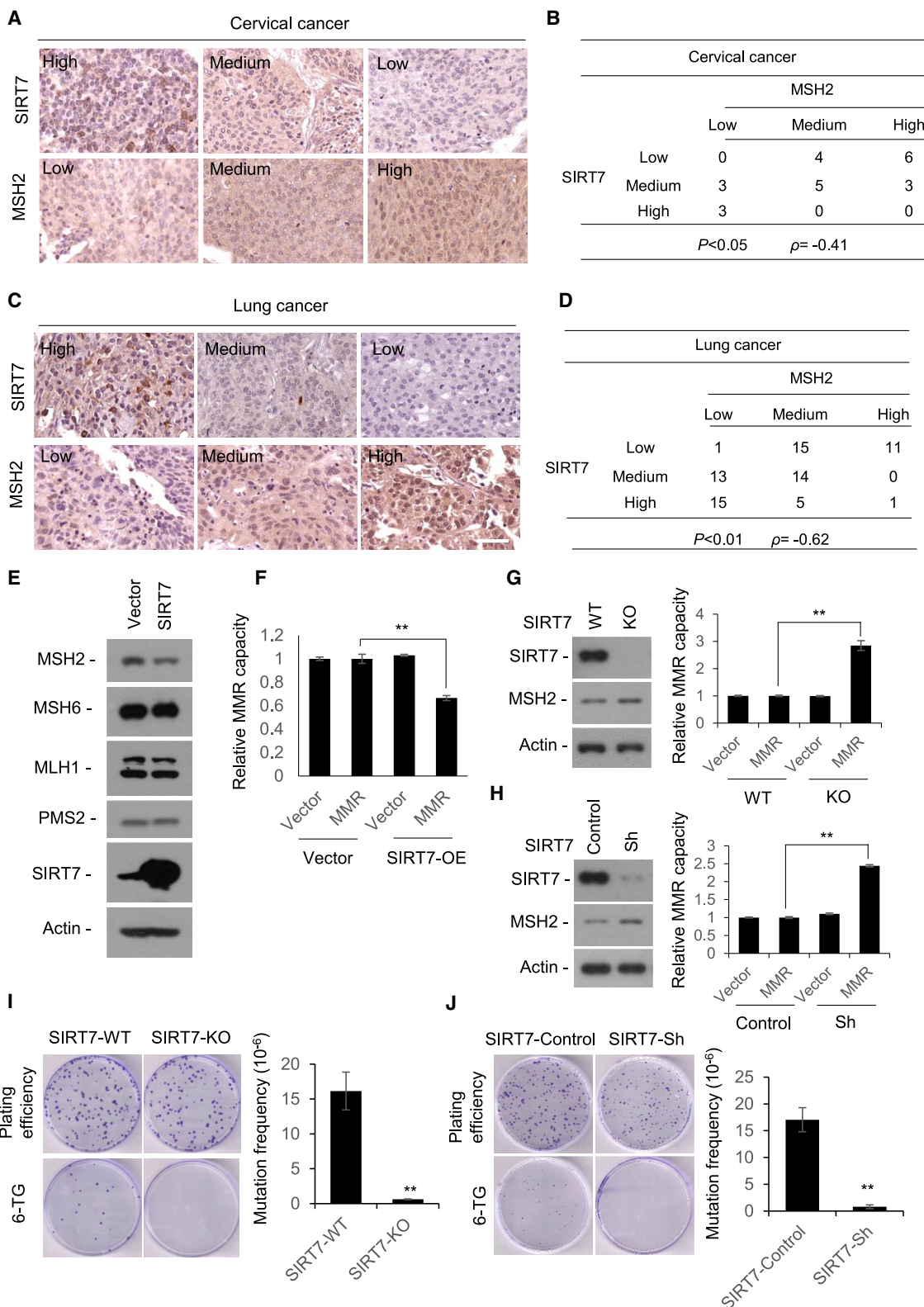
## INTRODUCTION

Genotoxic stress-induced apoptotic cell death by chemotherapy remains the core of anticancer treatment. However, resistance to genotoxic drugs is still a major obstacle for cancer therapy.<sup>1–3</sup> Microsatellite instability (MSI) has been a long-standing biomarker of genomic instability and a meaningful predictor for drug resistance.<sup>4</sup> High-frequency MSI is the hallmark of breast carcinoma, lung cancer, and Lynch syndrome due to mutations or deletions in one of the mismatch repair (MMR) genes.<sup>5–8</sup> The MMR system consists of MutS $\alpha$  (MSH2-MSH6) and MutS $\beta$  (MSH2-MSH3) complexes. MutS $\alpha$  recognizes single base-base mismatches and 1–2 nucleotide insertion/deletion mispairs, whereas MutS $\beta$  recognizes large insertion/deletion heteroduplexes. MMR plays an important role in the correction of DNA polymerase errors, either by preventing error-prone bypass replication or correcting the formed mismatches.<sup>9–11</sup> Defects or inactivation in MMR genes, such as MSH2, MLH1, MSH6, and PMS2, lead to unrepaired deletions in both mono- and dinucleotide repeats, resulting in variable lengths of these repeats and

MSI.<sup>12</sup> Notably, MMR also plays a linking role between cellular DNA damage and apoptosis initiation, while MSH2 overexpression induces apoptosis in the repair-deficient cells.<sup>13</sup> Interestingly, there are several studies that have demonstrated that MMR proteins are reduced under different drug treatments. Temozolomide (TMZ) treatment leads to a reduction in MSH2/MSH6 proteins in glioma cells.<sup>14</sup> Additionally, human colorectal cancer (CRC) cells show reduced levels of MMR proteins during epidermal growth factor receptor (EGFR)/BRAF inhibition, which triggers a shift from high-fidelity to error-prone DNA repair.<sup>15</sup> This shift increases the occurrence of MSI and contributes to drug resistance.<sup>16–19</sup> Nevertheless, how MMR is downregulated and how MSI is triggered during drug treatments remain unknown.

Deacetylase SIRT7, the only member of sirtuins (SIRT1–7) that localizes in the nucleoli, has drawn attention due to its central functions in cellular metabolism, stress response, genome stability, DNA repair, and drug resistance.<sup>20–24</sup> Within the nucleoli, SIRT7 regulates ribosomal DNA transcription by activating RNA polymerase I.<sup>25,26</sup> Our previous report demonstrated that SIRT7 is an energy sensor shuttling from the nucleoli to nucleoplasm





(legend on next page)

to prevent cell death in response to glucose starvation.<sup>27</sup> SIRT7 is elevated in human breast, thyroid, oral squamous, lung, and liver cancers. SIRT7 knockdown in cancer cell lines reduces cell growth and induces apoptosis.<sup>28–31</sup> In addition, SIRT7 depletion leads to increased p53-mediated apoptosis and a significantly diminished resistance to oxidative and genotoxic stress.<sup>32</sup> SIRT7-deficient mice exhibit genomic instability and phenotypes suggestive of premature aging, which may result from defective double-strand break (DSB) repair.<sup>33</sup> SIRT7 promotes DNA repair by H3K18 deacetylation at break sites, thereby influencing non-homologous end joining (NHEJ) repair efficiency.<sup>34</sup> SIRT7-catalyzed H3K122 desuccinylation is implemented in the DNA damage response and cell survival.<sup>35</sup> SIRT7 has recently been reported to be critical for the inactivation of ATM (ataxia-telangiectasia mutated serine/threonine kinase) activity and DNA damage repair.<sup>36</sup> Clearly, SIRT7 is involved in multiple signaling pathways to regulate the DNA damage response and cell death, but molecular factors and mechanisms that control SIRT7 chemotherapeutic resistance functions are largely unexplored.

Here, we report that DNA damage agents such as 6-thioguanine (6-TG), 6-mercaptopurine (6-MP), and etoposide induce MSI and that adaptive mutability in cervical tumor cells is SIRT7 dependent. Mechanistically, SIRT7 interacts and destabilizes MSH2, thereby leading to MMR impairment, MSI, and chemotherapy resistance. Moreover, DNA damage treatment triggers ATM kinase-dependent phosphorylation and subcellular relocalization of SIRT7. Our results reveal that ATM-dependent SIRT7 phosphorylation serves as a driving mechanism for MMR impairment and MSI following DNA-damaging treatment, suggesting that SIRT7 phosphorylation has potential as a target for increasing therapeutic effectiveness in tumors.

## RESULTS

### SIRT7 negatively correlates with MSH2 in human tumors

It was previously reported that SIRT7 is overexpressed in human cancers such as cervical cancer, lung cancer, bladder cancer, and CRC and related to drug resistance.<sup>37–42</sup> MSI status, the biomarker of drug resistance in cancer cells, is frequently triggered during DNA-damaging treatments.<sup>43</sup> To explore the correlation between SIRT7 protein level and MSI in tumors, we first examined MSI status in SIRT7 highly expressed tumors. As MSI is almost always associated with the defective MMR proteins MSH2, MSH6, MLH1, and PMS2, we performed immunohistochemistry staining of the MSH2 protein on tissue chips

of human cervical and lung cancers. The results revealed that there was a significantly high protein level of SIRT7 but a low protein level of MSH2 in human cervical cancer (Figures 1A and 1B) and lung cancer (Figures 1C and 1D) tumor tissues. Next, we detected these protein levels to assess MSI status in SIRT7-overexpressing cells. The result revealed that MSH2 protein was downregulated in SIRT7-overexpressing cells (Figure 1E). Given that MMR protein levels determine the MMR capacity, we used a quantitative MMR reporter assay to assess the MMR capacity in cells overexpressing SIRT7 and found that the MMR capacity was significantly decreased in these cells (Figure 1F). Conversely, we observed that in cells with SIRT7 knockdown or knockout (KO), the MSH2 protein level increased, and the MMR capacity was markedly enhanced (Figures 1G and 1H). Since MMR capacity directly affects microsatellite stability, we also performed microsatellite stability analysis in SIRT7-KO cells and found that SIRT7 KO significantly reduced the occurrence of MSI (Figure S1A). Additionally, we next explored whether SIRT7 affects adaptive mutability. The results showed that mutation frequency was decreased in SIRT7-KO cells (Figure 1I). Similar results were also observed in SIRT7-knockdown cells (Figure 1J). The above data suggest that the high expression of SIRT7 drives MMR impairment, MSI occurrence, and adaptive mutability in human cancers.

### SIRT7 interacts with MSH2 and impairs the MMR system

To better understand the role of SIRT7 in MSI occurrence, we examined the interaction between SIRT7 and MSH2. The mass spectrometry analysis identified MSH2 is a candidate binding protein of SIRT7 (Figures 2A and 2B; Table S1). Next, we found that SIRT7 interacted with MSH2 at both exogenous and endogenous levels (Figures 2C and 2D). The direct SIRT7-MSH2 association was verified *in vitro* (Figure 2E). Next, we examined whether SIRT7 regulates MutS $\alpha$  complex formation. The results showed that SIRT7 overexpression markedly attenuated the MSH2-MSH6 interaction (Figure 2F). Consistent with previous reports that the MSH2 level is maintained by forming MSH2-MSH6 or MSH2-MSH3 heterodimers, our results show that KO of SIRT7 enhances both the protein levels and stability of MSH2 (Figure 2G). Moreover, transient overexpression of SIRT7 increases MSH2 ubiquitination (Figure 2H), and treatment with proteasome inhibitor MG132 markedly attenuates SIRT7-overexpression-induced downregulation of MSH2 (Figure 2I). These results indicate that SIRT7 interacts with MSH2, leading to its degradation and, thereby, impairing the MMR system.

**Figure 1. SIRT7 negatively correlates with MSH2 in human tumors**

(A–D) Comparison of SIRT7 and MSH2 protein expression revealed by tissue array. Examples are shown of immunohistochemical images of tumor tissue in cervical (A) and lung (C) cancers stained with anti-SIRT7 and anti-MSH2 antibodies, respectively (scale bar, 50  $\mu$ m). Levels of SIRT7 and MSH2 expression were classified as high, medium, and low according to the staining signals in each group. Spearman's  $\rho$ -coefficient test was used for the evaluation of correlations between SIRT7 and MSH2 immunohistochemical expression status in cervical (B) and lung (D) cancer tissues.  $p < 0$  indicates a negative correlation. The level of signification is expressed by the  $p$  value.

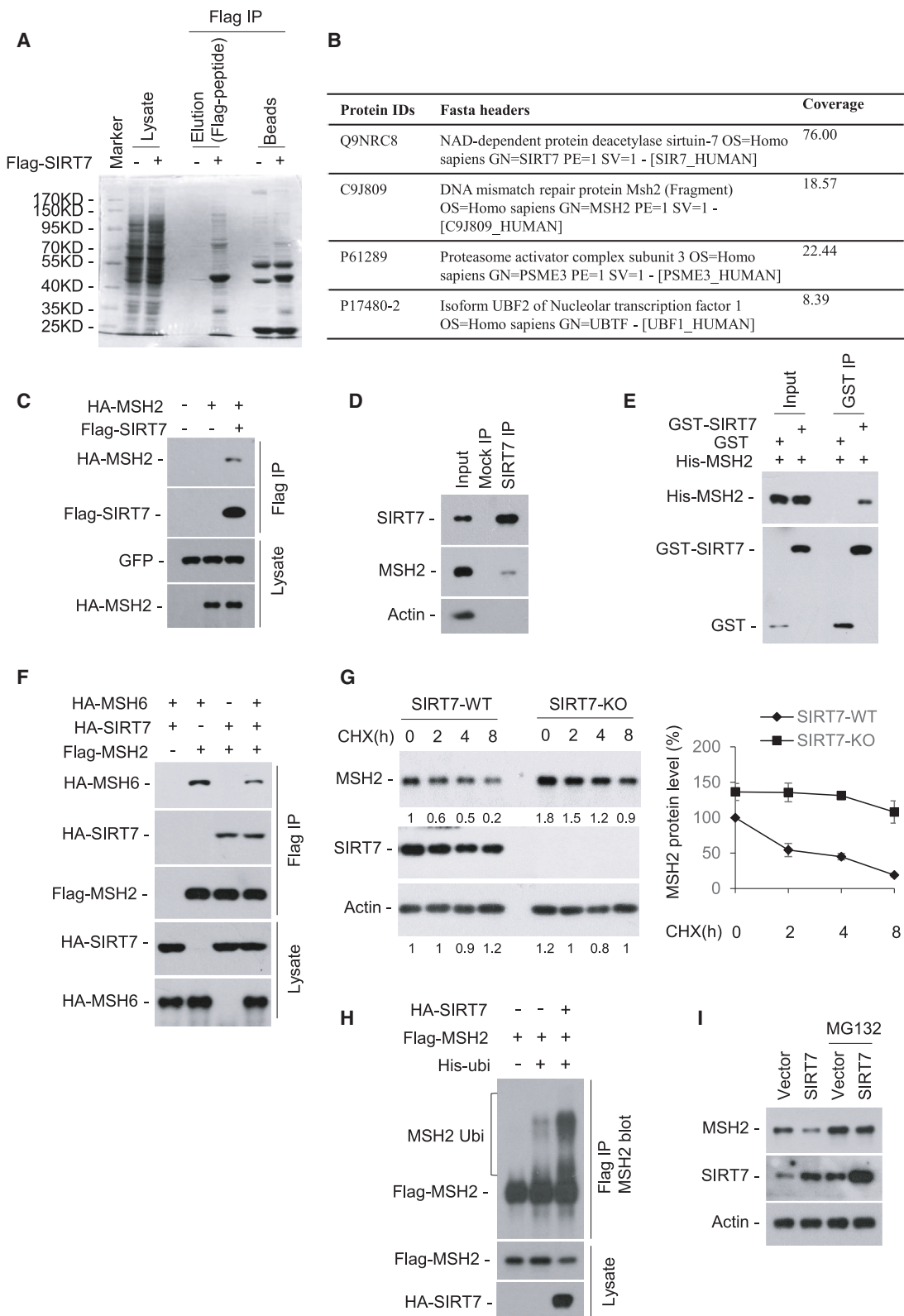
(E) Western blots of SIRT7-overexpressing (SIRT7-OE) HeLa cells using antibodies targeting MSH2, MSH6, MLH1, and PMS2, showing the expression of four MMR proteins.

(F) Relative MMR capacities in vector and SIRT7-OE HeLa cells.

(G and H) Relative MMR capacities in stable SIRT7-knockout (G) and -knockdown (H) HeLa cells. SIRT7 and MSH2 expression were blotted using antibodies targeting SIRT7 and MSH2.

(I and J) Mutability assay in stable SIRT7-knockout (I) and -knockdown (J) HeLa cells.

Data represent mean  $\pm$  SD;  $n = 3$  independent experiments; \*\* $p < 0.01$ ; Student's  $t$  test. See also Figure S1.



(legend on next page)

### SIRT7 destabilizes MSH2 via deacetylation

Previous studies identified that MSH2 is post-translationally modified by acetylation.<sup>17</sup> We therefore examined whether SIRT7 deacetylates MSH2. The results showed that only the wild type (WT), but not the enzymatic-inactive mutant (H187Y) of SIRT7 overexpression, markedly decreased the acetylation level of MSH2 (Figure 3A). We then set out to identify the acetylation sites in MSH2 by overexpressing MSH2 in 293T cells followed by mass spectrometry analyses. As shown in Figure 3B, both K845 and K882 were detected as potential acetylation sites. A previous study reported that K845 is one of the acetylation sites of MSH2 and that either acetylation-deficient K845R or acetylation-mimicking K845Q mutants decreased their binding affinity with MSH6.<sup>17</sup> Unlike MSH2-K845Q, we observed that the MSH2-K882Q acetylation-mimicking mutation increased its binding affinity with MSH6 compared with the WT (Figure 3C). In addition, mimicking deacetylation at K882 (K-to-R mutation, K882R) markedly increased the MSH2 degradation rate, whereas mimicking acetylation at K882 (K-to-Q mutation, K882Q) prolonged the half-life of MSH2 (Figure 3D). Moreover, the ubiquitination level of MSH2-K882R is stronger than that of MSH2-K882Q (Figure 3E). Next, we generated a polyclonal anti-MSH2-K882 acetylation antibody that specifically recognizes K882-acetylated MSH2 (Figure 3F). Using this MSH2-K882 acetylation antibody, we observed that MSH2-K882 acetylation increased dramatically in SIRT7-KO cells (Figure 3G). Notably, MSH2-K882 acetylation can be detected in multiple tumor cell types, suggesting that the role of MSH2 acetylation at K882 commonly exists in human tumors (Figure 3H). These results demonstrate that SIRT7 destabilizes MSH2 and impairs the MMR system via deacetylation at K882.

### DNA-damaging drugs induce SIRT7-dependent MSH2 deacetylation and downregulation

MSH2 deacetylation at K882 was then tested following DNA-damaging treatment. The results showed that treatment with DNA-damaging drugs such as 6-TG, 6-MP, or etoposide markedly increased the interaction and subcellular colocalization of SIRT7 with MSH2 (Figures 4A–4C and S2A–S2C). DNA-damaging agents also markedly decreased the MSH2-K882 acetylation (Figures 4D

and S2D). We next determined whether SIRT7 affects MSH2 expression during treatment with DNA-damaging drugs. As expected, MSH2 protein levels were significantly reduced in normal SIRT7 cells but remained unchanged in SIRT7-deficient cells after treatment with DNA-damaging drugs (Figures 4E, 4F, S2E, and S2F). The data suggest that MSH2 deacetylation and downregulation are SIRT7 dependent under DNA-damaging drugs.

### Deacetylation of MSH2 at K882 induces MSI and drug resistance

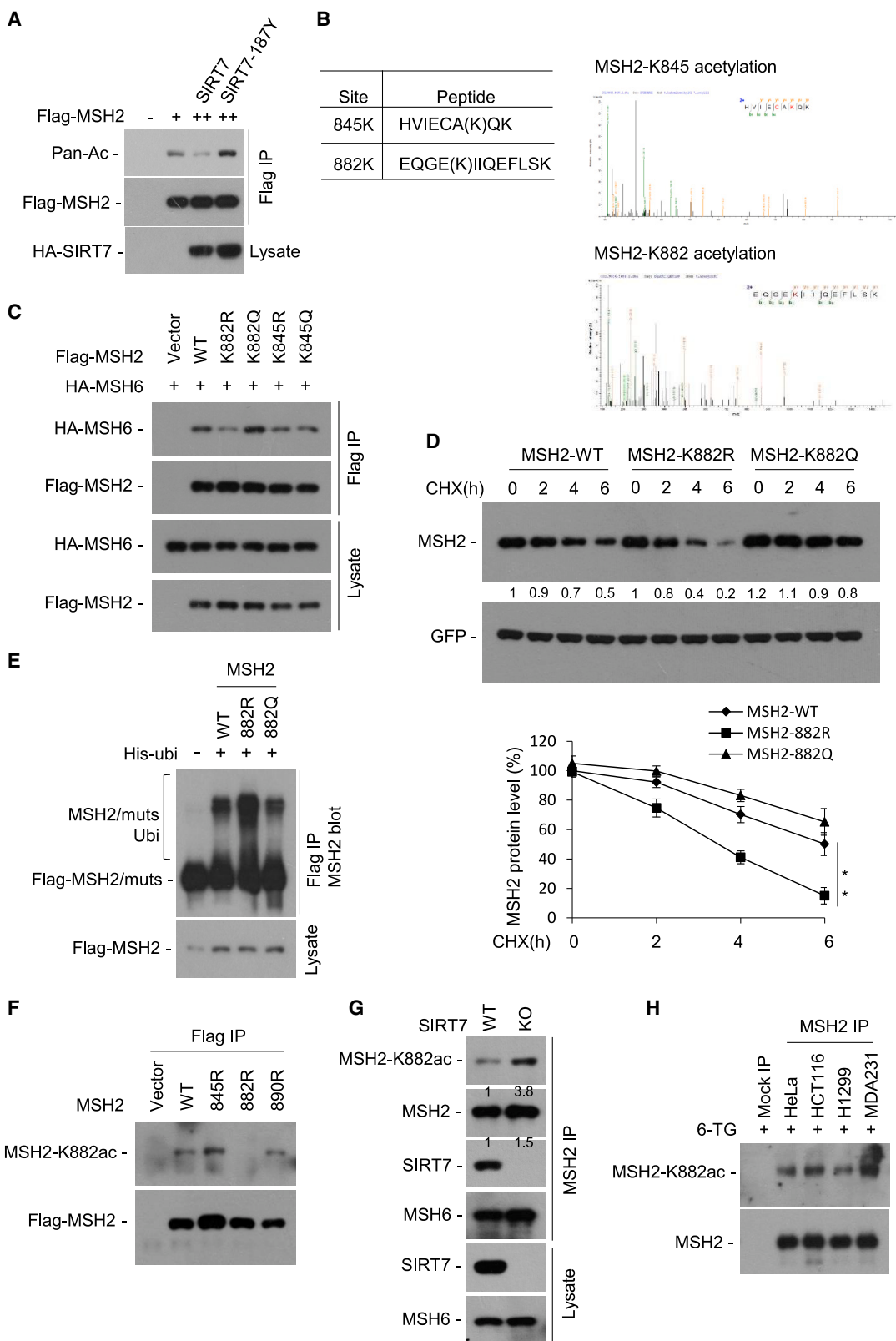
To examine the role of MSH2 deacetylation in MSI occurrence under the DNA-damaging treatment, stable MSH2-knockdown and FLAG-MSH2 (WT, K882R, or K882Q)-rescued cell lines were generated (Figure 5A). The results showed that MMR capacity was decreased and adaptive mutability frequency was increased in the MSH2-K882R-complemented cells after the 6-TG treatment (Figures 5B and 5C). In addition, we observed that MSH2 knockdown led to a marked reduction in 6-TG-induced cell death, while complementation of either MSH2-WT or -K882Q (but not MSH2-K882R) restored cell sensitivity to the 6-TG treatment (Figure 5D). Next, we tested whether MSH2 can enhance the therapeutic response of xenograft tumors in mice to the 6-TG treatment in an acetylation-dependent manner. The MSH2-WT-, K882R-, or K882Q-rescued cells were subcutaneously injected into nude mice above the left and right hind legs separately. The results showed that the tumor growth was markedly inhibited in the MSH2-WT- and K882Q- but not K882R-rescued groups receiving the 6-TG treatment (observed by a reduction in tumor volume; Figures 5E and 5F). These results demonstrate that the acetylation status of MSH2 at K882 by SIRT7 plays a crucial role in determining MSI occurrence and drug resistance.

### DNA damage induces SIRT7 phosphorylation and nucleoplasmic localization

SIRT7 is localized primarily in the nucleolus and colocalized with MSH2 in the nucleoplasm under DNA-damaging drug treatment. This fact motivated us to test SIRT7 redistribution following DNA-damaging stimuli. Interestingly, transiently expressed SIRT7 distributed throughout the nucleoplasm in response to DNA-damaging drugs (Figures 6A, 6B, S3A, and S3B). We have

### Figure 2. SIRT7 interacts with MSH2 and impairs the MMR system

- (A and B) Mass spectrometry analysis to identify potential SIRT7-interacting proteins. The 293T cells transfected with FLAG-SIRT7 plasmids were harvested and lysed, immunoprecipitated with FLAG-M2 beads, eluted with FLAG-peptide, and then subjected to SDS-PAGE and visualized using Coomassie blue staining (A). The immunoprecipitated proteins were detected by mass spectrometry assay; both MSH2 protein and the previous study have proved that SIRT7-interacting proteins such as PSME3 and UBF1 are identified (B).
- (C–E) SIRT7 interacts with MSH2.
- (C) FLAG-SIRT7 and HA-MSH2 were cotransfected into 293T cells, followed by immunoprecipitation (IP) using FLAG-M2 beads and western blot for MSH2 using anti-HA antibody. GFP was used as an external control and blotted using an anti-GFP antibody.
- (D) Endogenous SIRT7 in HeLa cells was precipitated using anti-SIRT7 antibody or immunoglobulin (Ig)G (mock IP), and coprecipitated MSH2 was detected by western blot.
- (E) SIRT7 interacts with MSH2 *in vitro*. Recombinant His-tagged MSH2 was incubated with GST-SIRT7 or GST proteins at 4°C for 4 h followed by GST pull-down and western blot.
- (F) SIRT7 inhibits MutS $\alpha$  (MSH2-MSH6) formation. FLAG-MSH2, HA-MSH6, and HA-SIRT7 plasmids were cotransfected to 293T cells, followed by IP using FLAG-M2 beads and western blot for MSH7 and SIRT7 using anti-HA antibody.
- (G) SIRT7 destabilizes MSH2. SIRT7-WT and -KO HeLa cells were treated with translation inhibitor cycloheximide (CHX; 50  $\mu$ g/mL). MSH2 protein was detected by western blot.
- (H) 293T cells transfected with His-ubiquitin, FLAG-MSH2, and HA-SIRT7 plasmids. Ubiquitinated proteins were precipitated using FLAG-M2 beads. MSH2 ubiquitination was detected by western blot using anti-MSH2 antibody.
- (I) Vector and SIRT7-OE stable HeLa cells were treated with MG132 (25  $\mu$ M, 4 h). MSH2 protein was detected by western blot.



(legend on next page)

previously reported that the phosphorylation status of SIRT7 plays a crucial role in determining its distribution, protein level, and interaction under glucose starvation.<sup>27</sup> Next, we tested whether phosphorylation is involved in DNA-damaging-drug-induced redistribution of SIRT7. As expected, SIRT7 phosphorylation increased under DNA-damaging drug treatments (Figure 6C). We performed mass spectrometric phosphopeptide analysis of purified FLAG-SIRT7 transiently expressed in 293T cells and identified S54, S166, and T284 within SIRT7 as potential phosphorylation sites.<sup>27</sup> We next generated phosphorylation-defective mutants (S/T to A) and phosphomimetic mutations (S/T to D/E) of these putative phosphorylation sites. Interestingly, transiently expressed SIRT7-S166D/E mutants distributed throughout the nucleoplasm, whereas other mutants still localized mainly in the nucleolus (Figure 6D). To further confirm SIRT7-S166 phosphorylation under DNA-damaging stress, we generated a SIRT7 phospho-S166-specific antibody (Figure 6E) and found that DNA-damaging drug treatment induced strong SIRT7 phosphorylation (Figures 6F and S3C). The data indicate that SIRT7 translocating to the nucleoplasm in response to DNA-damaging drugs is phosphorylation dependent and that the phosphorylation status of SIRT7 at S166 plays a crucial role in determining its subcellular redistribution.

### SIRT7-S166 phosphorylation induces MSI and drug resistance in an ATM-dependent manner

Notably, S166 is a highly conserved amino acid residue of SIRT7 in various mammalian species (Figure 6G), and the amino acid sequence around S166 of SIRT7 fits the ATM/ATR (ataxia telangiectasia and Rad3-related protein serine/threonine-protein kinase) phosphorylation consensus motif (pS/pTQ) (Figure 6H). To further confirm that SIRT7 is a substrate of ATM/ATR, we detected the phosphorylation of SIRT7 mutants using an ATM/ATR substrate phosphorylation antibody. The results showed that S166 is an ATM/ATR phosphorylation site (Figure 6I). DNA-damaging drug treatment dramatically increased ATM/ATR-dependent phosphorylation of SIRT7 (Figure 6J). To further detect whether SIRT7 is phosphorylated by the ATM or ATR kinase, we introduced inhibitors targeting ATM or ATR to treat cells and found that 6-TG-induced SIRT7 phosphorylation was diminished by ATM inhibitors or ATR inhibitors (Figure 6K). The WT ATM (ATM-WT), but not the kinase-dead mutant (ATM-DN), phosphorylated

SIRT7-S166 *in vitro* (Figure 6L). Moreover, the overexpression of ATM led to the downregulation of MSH2 protein levels in the SIRT7-WT cells but not the SIRT7-KO cells (Figure 6M). Furthermore, compared with the SIRT6-S166A mutant, overexpression of the SIRT7-S166D mutant markedly enhanced its binding to MSH2 coupled with a reduction of MSH2-K882 acetylation and MSH2-MSH6 binding (Figure 6N). These results suggest that ATM-dependent phosphorylation of SIRT7 at S166 plays a crucial role in regulating MMR and MSH2-K882 deacetylation.

### SIRT7 phosphorylation induces drug resistance via MSH2-K882 deacetylation

Next, we examined whether SIRT7-S166 phosphorylation regulates its activity in resistance to DNA-damaging drugs. The results showed that rescue SIRT7-S166D mutants, but not the SIRT7-S166A mutant, markedly attenuated cell death under 6-TG and 6-MP treatments (Figures 7A and S4A). In addition, we tested whether SIRT7 phosphorylation was involved in the therapeutic response of xenograft tumors in mice on drug treatment. SIRT7 knockdown HeLa cells rescued with SIRT7 WT/S166A/S166D were injected into nude mice subcutaneously above the left and right hind legs separately. The results showed that the xenograft tumors with SIRT7-S166A were more sensitive to 6-TG or etoposide than those of SIRT7-WT and -S166D (observed by a reduction of tumor volume) (Figures 7B, 7C, S4B, and S4C). The MSH2 staining and protein level of tumor sections identified that the SIRT7-S166D xenograft tumors showed a significant increase in MSI occurrence (Figures 7D and 7E). Similarly, after the etoposide treatment, SIRT7 knockdown led to MSH2 accumulation. Rescuing with the SIRT7-WT or S166D/E mutant markedly inhibited SIRT7-knockdown-induced MSH2 enhancement, whereas rescuing with SIRT7-S166A had no such result (Figure S4D).

To further examine the contribution of MSH2 acetylation to drug sensitivity in SIRT7-deficient cells under DNA-damaging stress, a stable SIRT7 and MSH2 double-knockdown and FLAG-MSH2 (WT, K882R, or K882Q)-rescued cell lines were generated (Figure 7F). Using these stable cell lines, cell viability assays showed that MSH2 knockdown attenuated SIRT7-depletion-induced drug sensitivity, while rescue of both MSH2-WT and MSH2-K882Q (but not MSH2-K882R) recovered their 6-TG sensitivity in the SIRT7 and MSH2 double-knockdown cells

---

### Figure 3. SIRT7 destabilizes MSH2 via deacetylation

- (A) SIRT7 deacetylates MSH2. FLAG-MSH2 and HA-SIRT7-WT or -H187Y plasmids were cotransfected to 293T cells, followed by immunoprecipitation (IP) using FLAG-M2 beads and western blot for acetylation of MSH2 using anti-pan-acetyl antibody.
- (B) Identification of potential acetylation sites of MSH2. Potential phosphorylation sites in MSH2 as revealed by mass spectrometry analysis are shown. The mass spectra of the MSH2 peptides acetylated at K845 and K882 are shown.
- (C) Deacetylation of MSH2 at K882 decreases MutS $\alpha$  formation. 293T cells were transfected with the indicated FLAG-MSH2 K882 mutant plasmids and HA-MSH6 for 24 h. Cell lysates were immunoprecipitated with FLAG-M2 beads, followed by western blot with anti-FLAG and anti-HA antibody.
- (D) 293T cells transfected with WT or mutant FLAG-MSH2 K882R/Q were treated with cycloheximide (CHX; 50  $\mu$ g/mL) and analyzed for MSH2 stability by western blot using anti-FLAG antibody. Data represent mean  $\pm$  SD; \*\* $p$  < 0.01; Student's t test.
- (E) FLAG-MSH2-WT and acetylation mutants (882R/882Q) and His-ubiquitin plasmids were transfected into 293T cells. MSH2 ubiquitination was detected by FLAG-M2 bead IP, followed by western blot using anti-MSH2 antibody.
- (F) Characterization of antibody against MSH2 acetylation at K882 or FLAG.
- (G) HeLa cells with a stable knockout of SIRT7 (KO) or control (WT) were immunoprecipitated using anti-MSH2 antibody (MSH2 IP). MSH2 acetylation was blotted with anti-acetyl-lysine antibody, and MSH6 was blotted with anti-MSH6 antibody.
- (H) HeLa, HCT116, H1299, and MBA-MD-231 cells were treated with 6-TG (10  $\mu$ M) for 12 h. Cell lysates were immunoprecipitated with MSH2 antibody, and the acetylation level of MSH2 was detected using anti-MSH2-K882ac antibody.

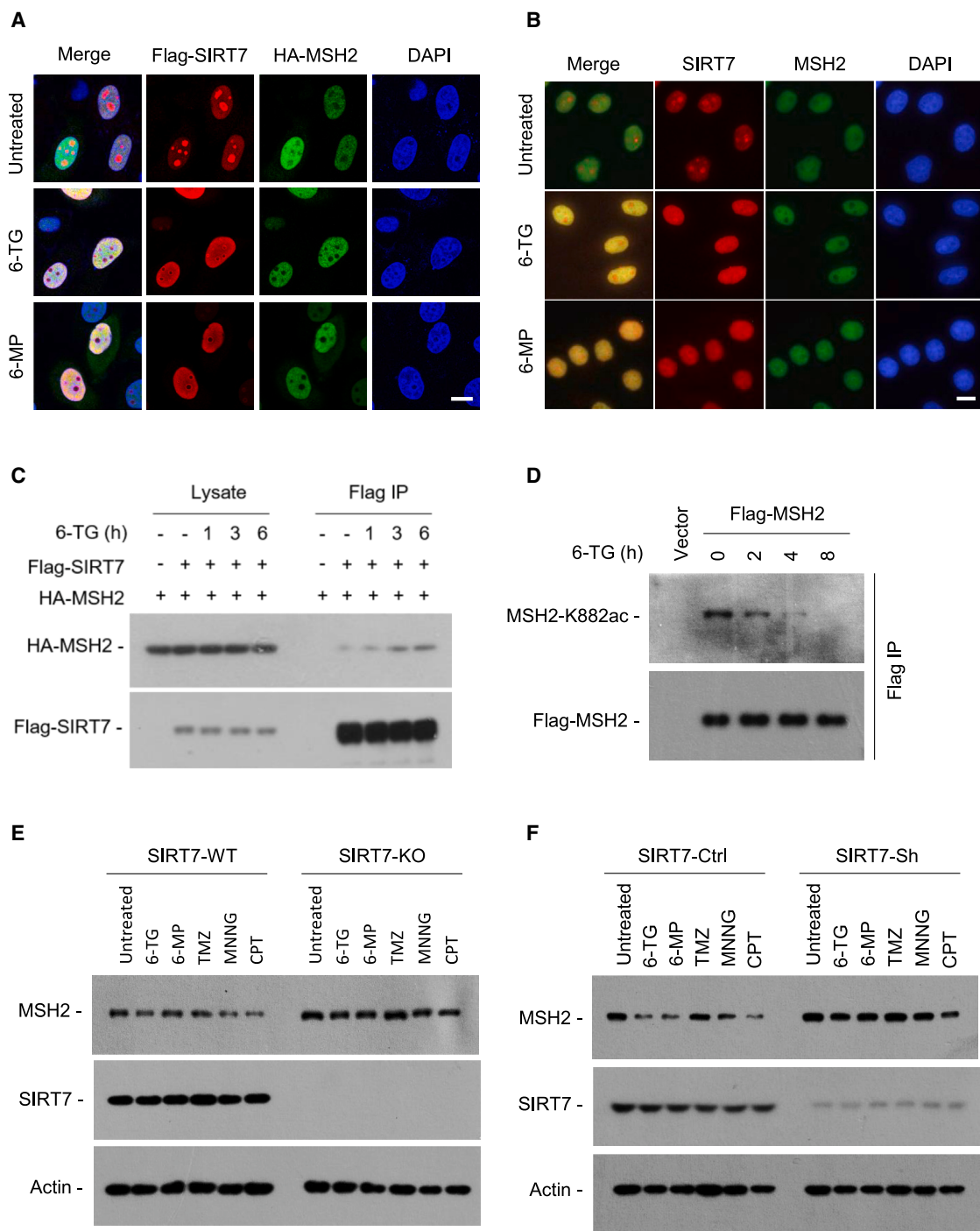


**Figure 4. DNA-damaging drugs induce SIRT7-dependent MSH2 deacetylation and downregulation**

(A and B) SIRT7 and MSH2 colocalization in nucleoplasm under drug treatment. FLAG-SIRT7 and HA-MSH2 were cotransfected in HeLa cells in the presence or absence of 6-TG (10  $\mu$ M) or 6-MP (10  $\mu$ M) treatment for 12 h. FLAG-SIRT7 was immunostained with anti-FLAG antibody (red), and HA-MSH2 was immunostained with anti-HA antibody (green) and visualized using fluorescence microscopy. Nuclei were stained with DAPI (scale bar, 10  $\mu$ m) (A). HeLa cells were treated with 6-TG (10  $\mu$ M) or 6-MP (10  $\mu$ M) treatment for 12 h. SIRT7 was immunostained with anti-SIRT7 antibody (red), and MSH2 was immunostained with anti-MSH2 antibody (green) and visualized using fluorescence microscopy. Nuclei were stained with DAPI (scale bar, 10  $\mu$ m) (B).

(C) 293T cells were transfected with FLAG-SIRT7 and HA-MSH2 and treated with 6-TG (10  $\mu$ M) for the indicated periods, followed by immunoprecipitation using anti-FLAG antibody and western blot with anti-HA antibody.

(legend continued on next page)

(Figure 7G). In addition, the above stable cells were injected into nude mice subcutaneously above the left and right hind legs separately. The xenograft tumors showed that SIRT7 depletion induced drug sensitivity, while rescue of both MSH2-WT and MSH2-K882Q (but not MSH2-K882R) recovered their 6-TG sensitivity in the SIRT7 and MSH2 double-knockdown cells (observed by a reduction of tumor volume) (Figures 7H and 7I). Collectively, these results indicate that SIRT7 phosphorylation at S166 contributes to DNA-damaging-drug-induced chemoresistance via deacetylation of MSH2 at K882.

## DISCUSSION

The present study demonstrates that SIRT7 downregulates the MMR protein MSH2 and triggers MSI in response to DNA-damaging stress. The data show that ATM-dependent SIRT7 phosphorylation at S166 redistributes to the nucleoplasm, interacts with and deacetylates MSH2, and thereby disassociates the MSH2-MSH6 complex, which leads to the chemotherapy resistance of tumor cells. Moreover, the rescue of the MSH2-K882Q acetylation-mimicking mutant in MSH2-knockdown stable cells can recover the effectiveness of drug-induced DNA damage in killing tumors *in vivo*. These findings present evidence that SIRT7 causes drug resistance induced by MMR protein downregulation or MSI occurrence during therapy, and SIRT7 phosphorylation at S166 has the potential to evaluate chemotherapy efficacy.

Our previous study revealed that SIRT7 is phosphorylated by AMPK at T153 and serves as a major mechanism to control SIRT7 redistribution and degradation under energy stress conditions. The present study observed that SIRT7 is also phosphorylated by ATM at S166 and is involved in MSH2-mediated chemoresistance, indicating that SIRT7 phosphorylation plays a predominant role in determining its subcellular location and function under different stress conditions. However, given that SIRT7 is a shuttle between nucleoli and the nucleoplasm, the present study does not elucidate how SIRT7 phosphorylation at S166 is accumulated in the nucleoplasm. Whether phosphorylated SIRT7 is anchored by other proteins in the nucleoplasm still needs to be elucidated. Because nucleoplasmic SIRT7 was found to have the ability to deacetylate MSH2, it will be interesting to identify new SIRT7-interacting proteins in the nucleoplasm under different stress conditions.

The present study also shows that ATM-induced phosphorylation and redistribution of SIRT7 lead to the chemoresistance of tumor cells, suggesting that mediating SIRT7 phosphorylation has the potential to improve tumor chemotherapy. A previous study revealed that SIRT7-mediated ATM deacetylation during the late stages of the DNA damage response is essential for its deactivation and DNA damage repair. In fact, ATM-SIRT7-positive feedback regulates the DNA damage response. On one hand, ATM is activated during DNA-damaging stress, followed

by SIRT7 phosphorylation and redistribution, which repress the MutS $\alpha$  complex via MSH2 and lead to cell survival. On the other hand, SIRT7 deacetylates ATM to deactivate it and prevent cell apoptosis. Accordingly, we believe that SIRT7 inhibition or mimic dephosphorylation is a determinant of the ATM-dependent resistance-to-apoptosis molecular switch.

The DNA damage repair capacity of cancer cells has a major influence on the efficiency of drug-induced DNA damage. DNA repair is crucial for the intrinsic response of tumors to chemotherapy. On the other hand, they are the reason for the resistance acquired during drug treatment. Based on this, tumor DNA repair defects may be complicated for chemotherapy. MMR or homologous repair (HR) deficiency confers tumor cells' sensitivity to DNA-damaging-inducing agents and, at the same time, causes genomic instability that promotes the acquisition of additional genetic alterations that may induce therapy resistance. Intriguingly, previous studies on SIRT7 in DNA damage repair have revealed that SIRT7 deacetylation of histone H3 lysine 18, which facilitates p53-binding protein 1 recruitment, promotes NHEJ repair while preventing HR. The present study shows that SIRT7 significantly represses the MMR system by deacetylating and downregulating MSH2 during DNA-damaging drug treatment, indicating that SIRT7 acts as a central hub in coordinating different DNA repair pathways and mediates a switch from high-fidelity to error-prone DNA damage repair. However, SIRT7 regulation in the crosstalk between MMR and other repair pathways during drug treatment should be further studied.

Notably, overexpressed SIRT7 protein expression has been observed in some types of tumors, such as cervical cancer, lung cancer, bladder cancer, and CRC, and is related to drug resistance.<sup>37–42</sup> Consistently, we showed that SIRT7 depletion induces cell death in response to drug-induced DNA damage. Moreover, SIRT7 triggers MSI in cancer cells during drug treatment. Combining these findings with the fact that SIRT7 deficiency significantly elevates MSH2 expression, we suggest that MSH2 deficiency (MSI)-mediated drug resistance is, at least in part, due to aberrant SIRT7 expression. Future clinical investigations of SIRT7 and MSI and their connection to chemotherapy resistance or sensitivity may provide more valuable information regarding the therapeutic strategy. In addition, we have examined the acetylation of MSH2-K882 in different types of tumor cells, such as HeLa, HCT116, H1299, and MBA-MD-231, and found that MSH2-K882 acetylation can be detected in multiple tumor cells, suggesting that MSH2-K882 acetylation exists in various tumor types. Therefore, the relationship between the expression level of SIRT7 and the acetylation level of the MSH2-K882 site in these tumors, as well as its correlation with chemotherapeutic resistance, is a topic that requires further investigation in the future.

Collectively, these results have revealed that SIRT7 acts as a driving force for MSI and that ATM-dependent phosphorylation of SIRT7 serves as a mechanism for inducing MMR impairment

(D) 293T cells transfected with FLAG-MSH2 were treated with 6-TG (10  $\mu$ M) for the indicated times, followed by immunoprecipitation using anti-FLAG antibody. Precipitated proteins were analyzed by western blot using anti-MSH2-K882ac antibody.

(E and F) Stable SIRT7-knockout (E) and -knockdown (F) HeLa cells were treated with 6-TG (1  $\mu$ M), 6-MP (1  $\mu$ M), TMZ (2  $\mu$ M), monomethylnitrosamine (MNNG; 2  $\mu$ M), or camptothecin (CPT; 200 nM) for 7 days. Western blots for these cells used an antibody targeting MSH2.

See also Figure S2.

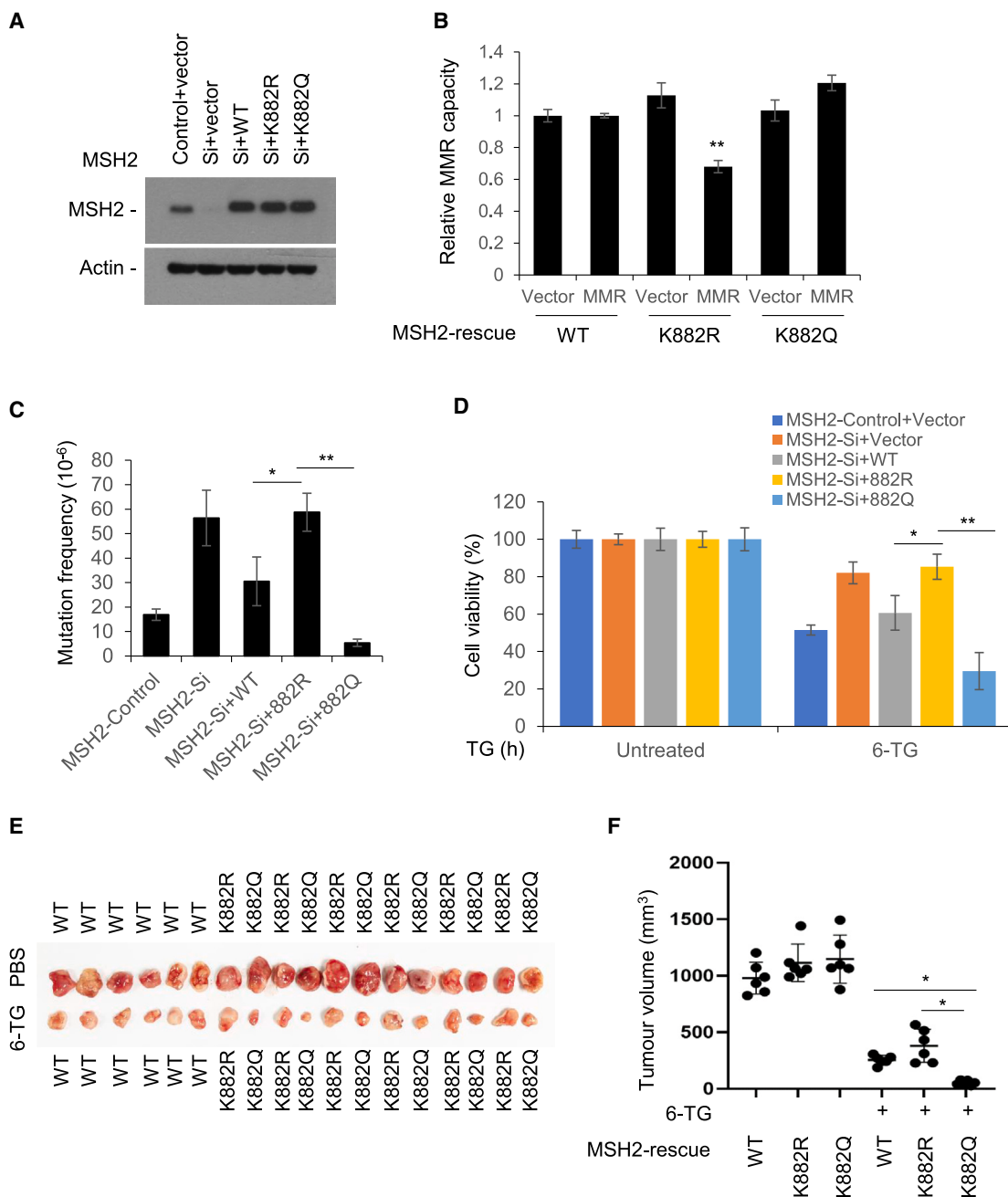


**Figure 5. MSH2-K882 deacetylation induces MSI and drug sensitivity**

(A) MSH2 knockdown (MSH2-Si) HeLa cells were recomplemented with RNAi-resistant MSH2-WT or -K882R/Q. Western blot shows MSH2 expression.

(B) Relative MMR capacities were detected in cells from (A).

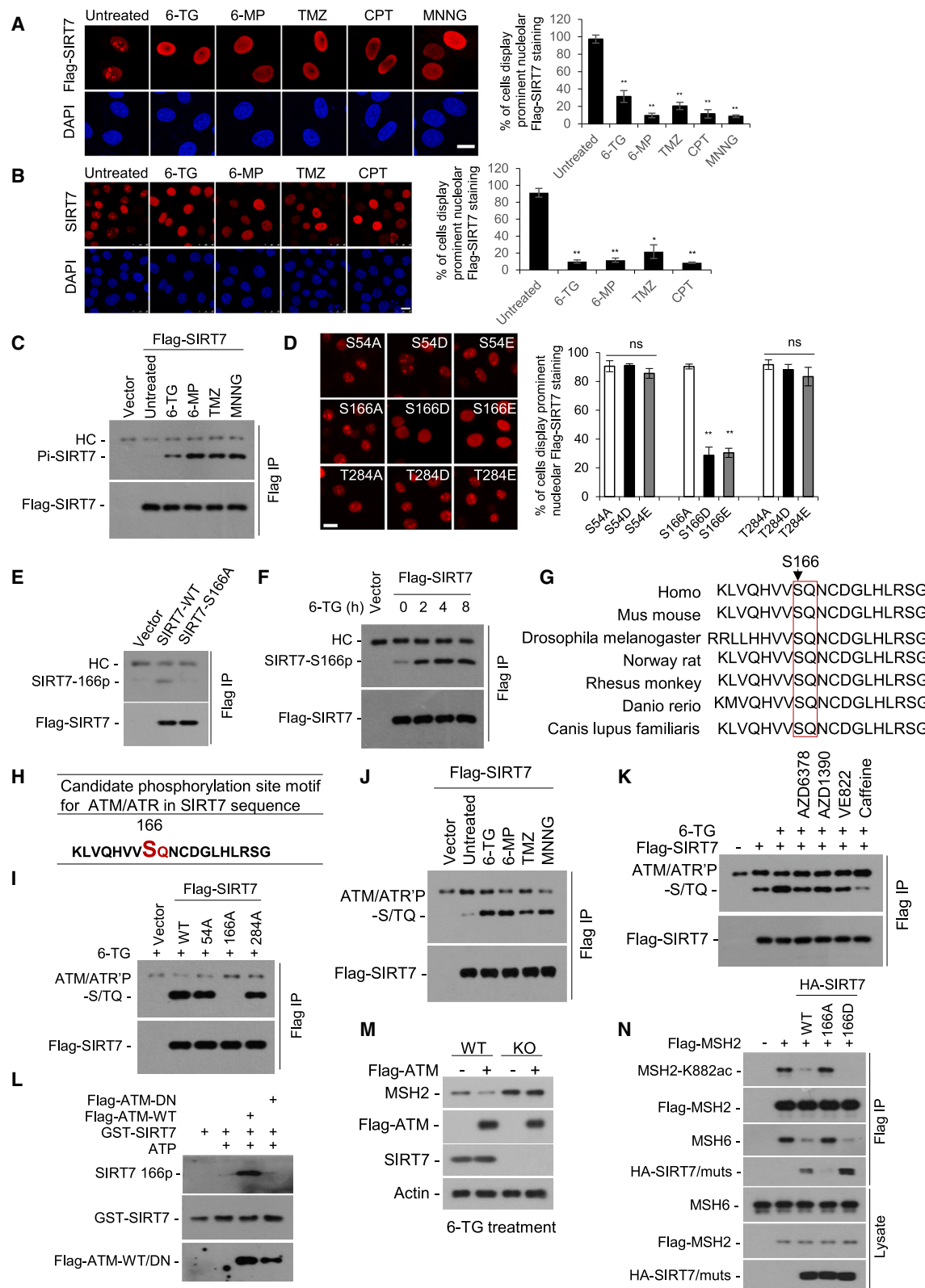
(C) Mutability frequency was detected in the cells from (A).

(D) Cells were treated with 6-TG (2  $\mu$ M) for 48 h, and apoptosis was analyzed by MTT assay.

(E and F) Mice with xenograft tumors originating from stable HeLa cells with rescue MSH2-WT, -882R, or -882Q were treated with 6-TG or PBS by intraperitoneal injection. Images show tumors after 32 days of PBS or 6-TG treatment (E). Tumor size was measured every 5 days, and tumor volume was calculated (F). Data represent mean  $\pm$  SD; \* $p$  < 0.05 and \*\* $p$  < 0.01; Student's t test.

and MSI following DNA-damaging treatment. Under DNA-damaging stress, SIRT7 is phosphorylated at S166 by ATM, redistributes to the nucleoplasm, interacts and deacetylates

MSH2, and, as a result, represses MSI-mediated cell death. The present study demonstrates that SIRT7 is a central hub in coordinating the transition between high-fidelity and error-prone



(legend on next page)

DNA repair pathways, as well as mediating the shift from apoptosis to resistance during chemotherapy. These results lead us to propose that SIRT7-S166 phosphorylation may be a potential marker for evaluating DNA-damaging drug effectiveness in tumor therapy.

#### Limitations of the study

This study has several limitations that should be acknowledged. First, the types of clinical tissue samples used in our study are somewhat limited. Although we demonstrated a negative correlation between SIRT7 and MSH2 in cervical and lung cancer tissue samples, SIRT7, as an oncogene, is highly expressed not only in cervical and lung cancers but also in other tumor types, such as colorectal and bladder cancers. Therefore, future work should involve increasing the diversity of clinical sample types to validate the correlation between SIRT7, MSH2, and MSI, which will help elucidate SIRT7's role as a biomarker for chemotherapy resistance in tumors. Second, we revealed that the acetylation modification of MSH2 at the K882 site regulates its stability and MMR capacity. However, the regulatory role of post-translational modifications of MSH2, particularly acetylation, is not a novel discovery, which limits the innovative contribution of our findings regarding MSH2's post-translational modifications. Third, our study lacks current omics data in the research techniques employed, such as single-cell sequencing of clinical tissue samples, spatial flow cytometry, and post-translational modifications of proteins. This limitation hinders our ability to

comprehensively understand the regulatory mechanisms of tumor resistance and does not take into account the heterogeneity of tumors. Additionally, while our research provides a thorough investigation of the molecular mechanisms, further exploration is needed in clinical applications. Our findings suggest that tumors with high SIRT7 expression can induce MSI through MSH2 under chemotherapy, and tumors with MSI often respond better to immunotherapy. Therefore, whether tumor cells with high SIRT7 expression are more responsive to PD-1 or PD-L1 immunotherapy is an important area for further research. Despite these limitations, the findings provide valuable insights and highlight areas for future research.

#### RESOURCE AVAILABILITY

##### Lead contact

Further information and requests for resources and reagents should be directed to and will be fulfilled by the lead contact, Chuangui Wang ([cgwang24@sdu.edu.cn](mailto:cgwang24@sdu.edu.cn)).

##### Materials availability

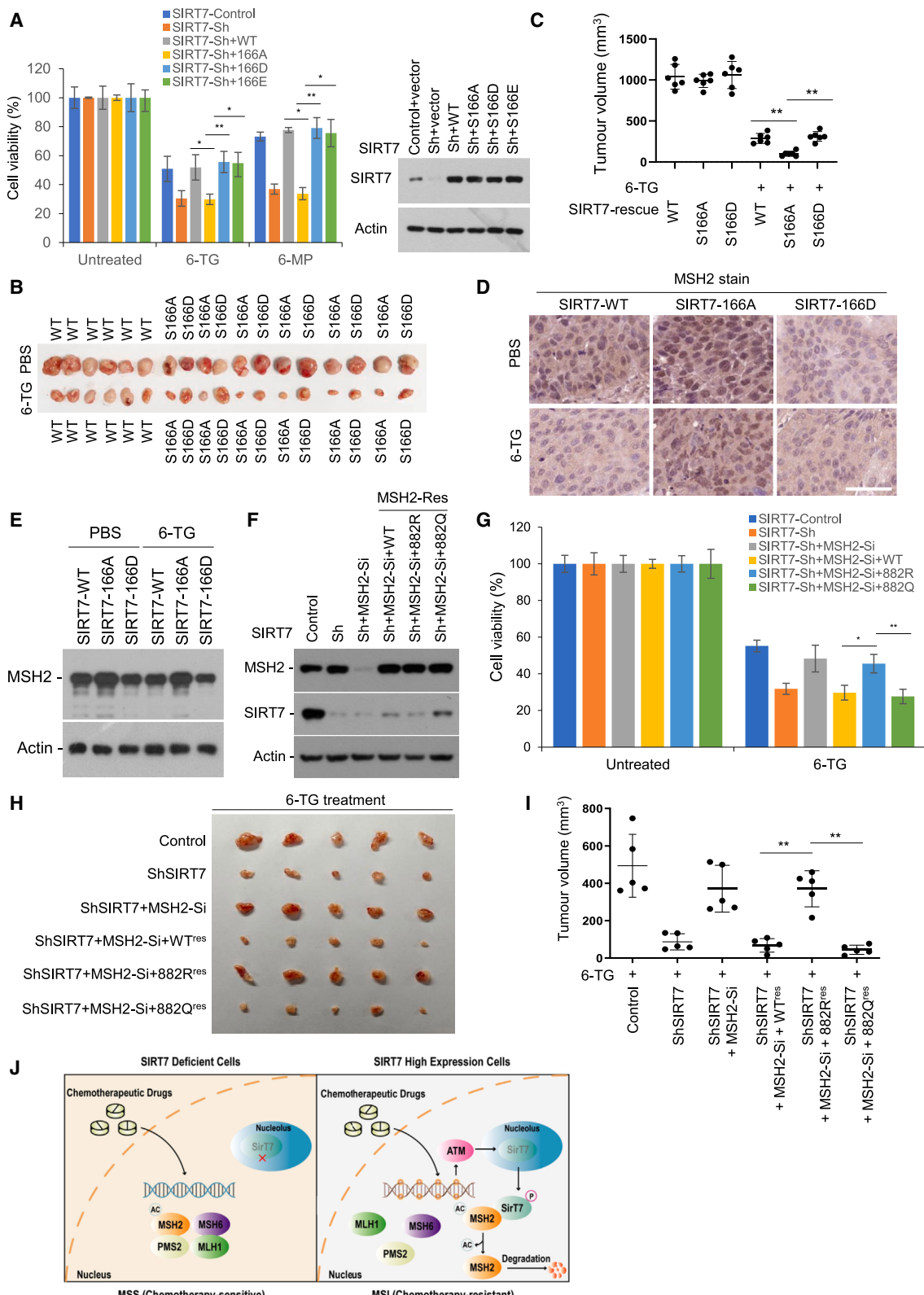
Two specific antibodies generated in this study, the anti-msh2-k882 acetylation antibody and anti-sirt7 phospho-s166 antibody, and all plasmids and stable cell lines generated in this study are available upon request to the [lead contact](#).

##### Data and code availability

- The mass spectrometry data have been deposited as [Table S1](#). These data are publicly available as of the date of publication.

#### Figure 6. DNA damage induces ATM-dependent SIRT7 nucleoplasmic localization and phosphorylation at S166

- (A and B) DNA-damaging stress induces SIRT7 nucleoplasmic redistribution. FLAG-SIRT7-transfected HeLa cells were treated with DNA-damaging stress (6-TG 10 μM/6-MP 10 μM/TMZ 20 μM/CPT 2 μM/MNNG 20 μM) for 12 h. FLAG-SIRT7 was immunostained with anti-FLAG antibody (red) and visualized using fluorescence microscopy (scale bar, 10 μm) (A). HeLa cells were treated with DNA-damaging stress (6-TG 10 μM/6-MP 10 μM/TMZ 20 μM/CPT 2 μM) for 12 h. SIRT7 was immunostained with anti-SIRT7 antibody (red) and visualized using fluorescence microscopy (scale bar, 10 μm) (B).
- (C) DNA-damaging stress induces SIRT7 phosphorylation. FLAG-SIRT7-transfected 293T cells were treated with DNA-damaging stress (6-TG 10 μM/6-MP 10 μM/TMZ 20 μM/MNNG 20 μM) for 4 h, followed by immunoprecipitation using FLAG-M2 beads and western blot for SIRT7 phosphorylation using anti-phospho-Ser/Thr antibody.
- (D) Subcellular location of SIRT7 mutants. HeLa cells transfected with FLAG-SIRT7-defective phosphorylation mutants (T/S to A) and mimicking phosphorylation mutants (T/S to D/E) were immunostained with anti-FLAG antibody (red) and visualized using fluorescence microscopy (scale bar, 10 μm).
- (E) Characterization of SIRT7 S166 phosphorylation antibody (SIRT7 S166p). Cell lysates from 293T cells transfected with the WT or mutant form of FLAG-SIRT7 were immunoprecipitated with FLAG-M2 beads, followed by western blot using antibodies against SIRT7 S166p or FLAG.
- (F) 293T cells transfected with FLAG-SIRT7 were treated with 6-TG (10 μM) for the indicated times. Cell lysates were immunoprecipitated with FLAG-M2 beads, followed by immunoblot with anti-SIRT7-S166p or anti-FLAG antibodies. HC, heavy chain.
- (G) SIRT7 Ser166 is highly conserved in mammals.
- (H) SIRT7 Ser166 is a potential conserved ATM/ATR motif site.
- (I) FLAG-SIRT7-WT or -S54A/S166A/T284A plasmid-transfected 293T cells were immunoprecipitated with anti-FLAG antibody, followed by immunoblot with anti-ATM/ATR substrate antibody.
- (J) DNA-damaging stress induces ATM-dependent SIRT7 phosphorylation. FLAG-SIRT7-transfected 293T cells were treated with DNA-damaging stress (6-TG 10 μM/6-MP 10 μM/TMZ 20 μM/CPT 2 μM/MNNG 20 μM), followed by immunoprecipitation using FLAG-M2 beads and western blot for SIRT7 phosphorylation using anti-ATM/ATR substrate-phospho antibody.
- (K) ATM activates SIRT7 phosphorylation under DNA-damaging stress. FLAG-SIRT7-transfected 293T cells were treated with 6-TG (10 μM, 4 h) in the presence or absence of ATM/ATR inhibitors (AZD6378 25 nM/AZD1390 20 nM/VE822 5 μM/caffeine 5 mM, 4 h), followed by immunoprecipitation using FLAG-M2 beads and western blot for SIRT7 phosphorylation using anti-ATM/ATR substrate-phospho antibody.
- (L) *In vitro* SIRT7 phosphorylation by activated ATM. GST-SIRT7 was expressed in *E. coli* and purified with GST beads. Activated FLAG-ATM or the kinase-dead mutant (ATM-DN) was precipitated from 6-TG (4 h)-treated FLAG-ATM or ATM-DN-overexpressing 293T cells using FLAG-M2 beads and eluted with FLAG peptide. GST-SIRT7 was incubated with or without FLAG-ATM or ATM-DN in the presence or absence of ATP as indicated. The reaction product was separated by SDS-PAGE and analyzed using western blot.
- (M) SIRT7-WT and -KO stable HeLa cells were transfected with FLAG-ATM. Cell lysates were subjected to western blot using anti-SIRT7, anti-FLAG, and anti-MSH2 antibodies.
- (N) 293T cells were transfected with FLAG-MSH2 and HA-SIRT7-WT/S166A/S166D, followed by immunoprecipitation using FLAG-M2 beads. Precipitated proteins were analyzed by western blot using anti-MSH2-K882ac antibody, anti-HA antibody, and anti-MSH6 antibody.
- See also [Figure S3](#).



(legend on next page)

- This paper does not report original code.
- Any additional information required to reanalyze the data reported in this paper is available from the [lead contact](#) upon request.

## ACKNOWLEDGMENTS

This work was supported by the National Natural Science Foundation of China (32170784, 32170707, 32470803, and 32070770).

## AUTHOR CONTRIBUTIONS

L.S., G.F., and Z.Z. performed most of the experiments; S.Z. and C.W. interpreted the data and wrote the manuscript; Xiaoyu Zhang, D.C., T.Z., J.G., Xiaoxia Zhang, M.L., C.H., J.Z., and M.W. helped with all experiments; and L.C., M.Z., and B.H. supervised the study and reviewed the manuscript. All authors have read and approved the final manuscript.

## DECLARATION OF INTERESTS

The authors declare no competing interests.

## STAR★METHODS

Detailed methods are provided in the online version of this paper and include the following:

- KEY RESOURCES TABLE
- EXPERIMENTAL MODEL AND SUBJECT DETAILS
  - Cell culture and plasmids
  - Animal studies
- METHOD DETAILS
  - Immunoprecipitation and western blotting
  - Immunofluorescence staining
  - Cell death analyses
  - Mass spectrometry analysis
  - MMR assay
  - Mutability assay
  - Tissue microarray and IHC staining
  - Microsatellite instability assay
- QUANTIFICATION AND STATISTICAL ANALYSES

## SUPPLEMENTAL INFORMATION

Supplemental information can be found online at <https://doi.org/10.1016/j.celrep.2025.115269>.

Received: July 9, 2024  
Revised: December 3, 2024  
Accepted: January 15, 2025  
Published: February 4, 2025

## REFERENCES

- Bouwman, P., and Jonkers, J. (2012). The effects of deregulated DNA damage signalling on cancer chemotherapy response and resistance. *Nat. Rev. Cancer* 12, 587–598.
- Holohan, C., Van Schaeybroeck, S., Longley, D.B., and Johnston, P.G. (2013). Cancer drug resistance: an evolving paradigm. *Nat. Rev. Cancer* 13, 714–726.
- Sancar, A., Lindsey-Boltz, L.A., Unsal-Kaçmaz, K., and Linn, S. (2004). Molecular mechanisms of mammalian DNA repair and the DNA damage checkpoints. *Annu. Rev. Biochem.* 73, 39–85.
- Gay, C.M., Parseghian, C.M., and Byers, L.A. (2020). This Is Our Cells Under Pressure: Decreased DNA Damage Repair in Response to Targeted Therapies Facilitates the Emergence of Drug-Resistant Clones. *Cancer Cell* 37, 5–7.
- Sargent, D.J., Marsoni, S., Monges, G., Thibodeau, S.N., Labianca, R., Hamilton, S.R., French, A.J., Kabat, B., Foster, N.R., Torri, V., et al. (2010). Defective mismatch repair as a predictive marker for lack of efficacy of fluorouracil-based adjuvant therapy in colon cancer. *J. Clin. Oncol.* 28, 3219–3226.
- Poulogiannis, G., Frayling, I.M., and Arends, M.J. (2010). DNA mismatch repair deficiency in sporadic colorectal cancer and Lynch syndrome. *Histopathology* 56, 167–179.
- Hiroaki Murata, N.H.K., Kang, Y., Gu, L., and Li, G.-M. (2002). Genetic and epigenetic modification of mismatch repair genes hMSH2 and hMLH1 in sporadic breast cancer with microsatellite instability. *Oncogene* 21, 5696–5703.
- Kim, W.S., Park, C., Hong, S.K., Park, B.K., Kim, H.S., and Park, K. (2000). Microsatellite instability(MSI) in non-small cell lung cancer(NSCLC) is highly associated with transforming growth factor-beta type II receptor(TGF-beta RII) frameshift mutation. *Anticancer Res.* 20, 1499–1502.
- Shen, K., Ye, Y., Jiang, K., Liang, B., Yang, X., and Wang, S. (2012). MSH2 is required for cell proliferation, cell cycle control and cell invasiveness in colorectal cancer cells. *Chin. Sci. Bull.* 57, 2580–2585.
- Brown, K.D., Rathi, A., Kamath, R., Beardsley, D.I., Zhan, Q., Mannino, J.L., and Baskaran, R. (2003). The mismatch repair system is required for S-phase checkpoint activation. *Nat. Genet.* 33, 80–84.

## Figure 7. SIRT7 phosphorylation induces drug resistance via MSH2-K882 deacetylation

- (A) SIRT7-WT/166A/166D/166E were rescued in stable SIRT7-knockdown cells and treated with 6-TG (2 μM) for 48 h. Cell viability was determined using the MTT assay. Western blots show SIRT7 expression.
- (B and C) Mice with xenograft tumors originating from stable HeLa cells with rescue SIRT7-WT, -S166A, or -S166D were treated with 6-TG (20 mg/kg) or PBS by intraperitoneal injection. Images show tumors after 32 days of PBS or 6-TG treatment. The tumor volume was calculated.
- (D) Immunohistochemistry of tumor sections from xenograft tumors using antibody targeting MSH2 shows expression of MMR proteins in tumor cells (scale bar, 50 μm).
- (E) Western blot of tumor sections from xenograft tumors using antibody targeting MSH2 shows expression of MMR proteins in tumor cells.
- (F and G) Stable SIRT7-control and -Sh HeLa cells infected with or without MSH2 knockdown lentivirus followed by complementary MSH2-WT or MSH2-K882R/Q lentivirus were treated with 6-TG (10 μM) for 48 h. Cell viability was determined using the MTT assay. Western blots show SIRT7 and MSH2 expression.
- (H and I) Mice with xenograft tumors originated from cells with stable SIRT7-control and -Sh HeLa cells rescued with or without MSH2 knockdown (MSH2-Si), followed by complementary MSH2-WT or MSH2-K882R/Q, were treated with 6-TG (20 mg/kg) or PBS by intraperitoneal injection. Images show tumors after 32 days of PBS or 6-TG treatment. The tumor volume was calculated.
- (J) Model showing how SIRT7 regulates MMR system to induce drug resistance. In SIRT7-deficient cells, MSH2 interacts with MSH6 to form the MutSα complex to keep microsatellite stability (MSS) and sensitize to DNA-damaging drugs. In high-SIRT7-expression cells, DNA-damaging drugs stimulate ATM-dependent SIRT7-S166 phosphorylation, which causes SIRT7 nucleoplasmic redistribution, SIRT7-MSH2 association, and MSH2 deacetylation, thus leading to MMR impairment, MSI, and drug resistance.
- Data represent mean ± SD; \*p < 0.05 and \*\*p < 0.01; Student's t test. MMR, mismatch repair; 6-TG, 6-thioguanine; 6-MP, 6-mercaptopurine; CPT, camptothecin; TMZ, temozolomide; MNNG, monomethylnitrosamine. See also [Figure S4](#).

11. Lv, L., Wang, F., Ma, X., Yang, Y., Wang, Z., Liu, H., Li, X., Liu, Z., Zhang, T., Huang, M., et al. (2013). Mismatch repair protein MSH2 regulates translesion DNA synthesis following exposure of cells to UV radiation. *Nucleic Acids Res.* **41**, 10312–10322.
12. Hoguen Kim, J.J., Vogelstein, B., and Hamilton, S.R. (1994). Clinical and pathological characteristics of sporadic colorectal carcinomas with DNA replication errors in microsatellite sequences. *Amer. J. Pathol.* **145**, 148–156.
13. Mastroloca, A.S., and Heinen, C.D. (2010). Nuclear reorganization of DNA mismatch repair proteins in response to DNA damage. *DNA Repair* **9**, 120–133.
14. McFadie-Figueroa, J.L., Braun, C.J., Stanciu, M., Nagel, Z.D., Mazzucato, P., Sangaraju, D., Cerniauskas, E., Barford, K., Vargas, A., Chen, Y., et al. (2015). Minor Changes in Expression of the Mismatch Repair Protein MSH2 Exert a Major Impact on Glioblastoma Response to Temozolomide. *Cancer Res.* **75**, 3127–3138.
15. Russo, M., Crisafulli, G., Sogari, A., Reilly, N.M., Arena, S., Lamba, S., Bartolini, A., Magri, A., Magri, A., Novara, L., et al. (2019). Adaptive mutability of colorectal cancers in response to targeted therapies. *Science* **366**, 1473–1480.
16. Ahmad, Y., Boisvert, F.M., Gregor, P., Cobley, A., and Lamond, A.I. (2009). NOPdb: Nucleolar Proteome Database—2008 update. *Nucleic Acids Res.* **37**, D181–D184.
17. Zhang, M., Xiang, S., Joo, H.Y., Wang, L., Williams, K.A., Liu, W., Hu, C., Tong, D., Haakenson, J., Wang, C., et al. (2014). HDAC6 deacetylates and ubiquitinates MSH2 to maintain proper levels of MutSalpha. *Mol. Cell* **55**, 31–46.
18. Diouf, B., Cheng, Q., Krynetskaia, N.F., Yang, W., Cheok, M., Pei, D., Fan, Y., Cheng, C., Krynetskiy, E.Y., Geng, H., et al. (2011). Somatic deletions of genes regulating MSH2 protein stability cause DNA mismatch repair deficiency and drug resistance in human leukemia cells. *Nat. Med.* **17**, 1298–1303.
19. Ting, S., Mairinger, F.D., Hager, T., Welter, S., Eberhardt, W.E., Wohlschlaeger, J., Schmid, K.W., Christoph, D.C., and ERCC1, M.L.H.1 (2013). MSH2, MSH6, and bettaII-tubulin: resistance proteins associated with response and outcome to platinum-based chemotherapy in malignant pleural mesothelioma. *Clin. Lung Cancer* **14**, 558–567.e3.
20. Li, W., Sun, Z., Chen, C., Wang, L., Geng, Z., and Tao, J. (2018). Sirtuin7 has an oncogenic potential via promoting the growth of cholangiocarcinoma cells. *Biomed. Pharmacother.* **100**, 257–266.
21. Choi, J.E., and Mostoslavsky, R. (2014). Sirtuins, metabolism, and DNA repair. *Curr. Opin. Genet. Dev.* **26**, 24–32.
22. de Oliveira, M.V.M., Andrade, J.M.O., Paraíso, A.F., and Santos, S.H.S. (2013). Sirtuins and cancer: new insights and cell signaling. *Cancer Invest.* **31**, 645–653.
23. Vazquez, B.N., Thackray, J.K., and Serrano, L. (2017). Sirtuins and DNA damage repair: SIRT7 comes to play. *Nucleus* **8**, 107–115.
24. Barber, M.F., Michishita-Kioi, E., Xi, Y., Tasselli, L., Kioi, M., Moqtaderi, Z., Tennen, R.I., Paredes, S., Young, N.L., Chen, K., et al. (2012). SIRT7 links H3K18 deacetylation to maintenance of oncogenic transformation. *Nature* **487**, 114–118.
25. Grob, A., Roussel, P., Wright, J.E., McStay, B., Hernandez-Verdun, D., and Sirri, V. (2009). Involvement of SIRT7 in resumption of rDNA transcription at the exit from mitosis. *J. Cell Sci.* **122**, 489–498.
26. Ford, E., Voit, R., Liszt, G., Magin, C., Grummt, I., and Guarente, L. (2006). Mammalian Sir2 homolog SIRT7 is an activator of RNA polymerase I transcription. *Genes Dev.* **20**, 1075–1080.
27. Sun, L., Fan, G., Shan, P., Qiu, X., Dong, S., Liao, L., Yu, C., Wang, T., Gu, X., Li, Q., et al. (2016). Regulation of energy homeostasis by the ubiquitin-independent REGgamma proteasome. *Nat. Commun.* **7**, 12497.
28. Li, H., Tian, Z., Qu, Y., Yang, Q., Guan, H., Shi, B., Ji, M., and Hou, P. (2019). SIRT7 promotes thyroid tumorigenesis through phosphorylation and activation of Akt and p70S6K1 via DBC1/SIRT1 axis. *Oncogene* **38**, 345–359.
29. Li, W., Zhu, D., and Qin, S. (2018). SIRT7 suppresses the epithelial-to-mesenchymal transition in oral squamous cell carcinoma metastasis by promoting SMAD4 deacetylation. *J. Exp. Clin. Cancer Res.* **37**, 148.
30. Shi, H., Ji, Y., Zhang, D., Liu, Y., and Fang, P. (2016). MicroRNA-3666-induced suppression of SIRT7 inhibits the growth of non-small cell lung cancer cells. *Oncol. Rep.* **36**, 3051–3057.
31. Zhao, J., Wozniak, A., Adams, A., Cox, J., Vittal, A., Voss, J., Bridges, B., Weinman, S.A., and Li, Z. (2019). SIRT7 regulates hepatocellular carcinoma response to therapy by altering the p53-dependent cell death pathway. *J. Exp. Clin. Cancer Res.* **38**, 252.
32. Vakhrusheva, O., Smolka, C., Gajawada, P., Kostin, S., Boettger, T., Kubin, T., Braun, T., and Bober, E. (2008). Sirt7 increases stress resistance of cardiomyocytes and prevents apoptosis and inflammatory cardiomyopathy in mice. *Circ. Res.* **102**, 703–710.
33. Song, C., Hotz-Wagenblatt, A., Voit, R., and Grummt, I. (2017). SIRT7 and the DEAD-box helicase DDX21 cooperate to resolve genomic R loops and safeguard genome stability. *Genes Dev.* **31**, 1370–1381.
34. Zhang, P.Y., Li, G., Deng, Z.J., Liu, L.Y., Chen, L., Tang, J.Z., Wang, Y.Q., Cao, S.T., Fang, Y.X., Wen, F., et al. (2016). Dicer interacts with SIRT7 and regulates H3K18 deacetylation in response to DNA damaging agents. *Nucleic Acids Res.* **44**, 3629–3642.
35. Li, L., Shi, L., Yang, S., Yan, R., Zhang, D., Yang, J., He, L., Li, W., Yi, X., Sun, L., et al. (2016). SIRT7 is a histone desuccinylase that functionally links to chromatin compaction and genome stability. *Nat. Commun.* **7**, 12235.
36. Tang, M., Li, Z., Zhang, C., Lu, X., Tu, B., Cao, Z., Li, Y., Chen, Y., Jiang, L., Wang, H., et al. (2019). SIRT7-mediated ATM deacetylation is essential for its deactivation and DNA damage repair. *Sci. Adv.* **5**, eaav1118.
37. Yu, H., Ye, W., Wu, J., Meng, X., Liu, R.Y., Ying, X., Zhou, Y., Wang, H., Pan, C., and Huang, W. (2014). Overexpression of sirt7 exhibits oncogenic property and serves as a prognostic factor in colorectal cancer. *Clin. Cancer Res.* **20**, 3434–3445.
38. Tang, M., Lu, X., Zhang, C., Du, C., Cao, L., Hou, T., Li, Z., Tu, B., Cao, Z., Li, Y., et al. (2017). Downregulation of SIRT7 by 5-fluorouracil induces radiosensitivity in human colorectal cancer. *Theranostics* **7**, 1346–1359.
39. Aljada, A., Saleh, A.M., and Al Suwaidan, S. (2014). Modulation of insulin/IGFs pathways by sirtuin-7 inhibition in drug-induced chemoresistance. *Diagn. Pathol.* **9**, 94.
40. Yu, J., Yuan, S., Song, J., and Yu, S. (2023). USP39 interacts with SIRT7 to promote cervical squamous cell carcinoma by modulating autophagy and oxidative stress via FOXM1. *J. Transl. Med.* **21**, 807.
41. Kumari, P., Tarighi, S., Fuchshuber, E., Li, L., Fernández-Duran, I., Wang, M., Ayoson, J., Castelló-García, J.M., Gámez-García, A., Espinosa-Alcantud, M., et al. (2024). SIRT7 promotes lung cancer progression by destabilizing the tumor suppressor ARF. *Proc. Natl. Acad. Sci. USA* **121**, e2409269121.
42. Ianni, A., Kumari, P., Tarighi, S., Braun, T., and Vaquero, A. (2024). SIRT7: a novel molecular target for personalized cancer treatment? *Oncogene* **43**, 993–1006.
43. Russo, M., Crisafulli, G., Sogari, A., Reilly, N.M., Arena, S., Lamba, S., Bartolini, A., Amodio, V., Magri, A., Novara, L., et al. (2019). Adaptive mutability of colorectal cancers in response to targeted therapies. *Science* **10**, 1126.
44. Hu, C., Zhang, S., Gao, X., Gao, X., Xu, X., Lv, Y., Zhang, Y., Zhu, Z., Zhang, C., Li, Q., et al. (2012). Roles of Kruppel-associated Box (KRAB)-associated Co-repressor KAP1 Ser-473 Phosphorylation in DNA Damage Response. *J. Biol. Chem.* **287**, 18937–18952.
45. Shen, J., Ju, Z., Zhao, W., Wang, L., Peng, Y., Ge, Z., Nagel, Z.D., Zou, J., Wang, C., Kapoor, P., et al. (2018). ARID1A deficiency promotes mutability and potentiates therapeutic antitumor immunity unleashed by immune checkpoint blockade. *Nat. Med.* **24**, 556–562.
46. Nagel, Z.D., Margulies, C.M., Chaim, I.A., McRee, S.K., Mazzucato, P., Ahmad, A., Abo, R.P., Butty, V.L., Forget, A.L., and Samson, L.D. (2014).

- Multiplexed DNA repair assays for multiple lesions and multiple doses via transcription inhibition and transcriptional mutagenesis. *Proc. Natl. Acad. Sci. USA* **111**, E1823–E1832.
47. Li, F., Mao, G., Tong, D., Huang, J., Gu, L., Yang, W., and Li, G.-M. (2013). The histone mark H3K36me3 regulates human DNA mismatch repair through its interaction with MutS $\alpha$ . *Cell* **153**, 590–600.
48. Fan, G., Sun, L., Shan, P., Zhang, X., Huan, J., Zhang, X., Li, D., Wang, T., Wei, T., Zhang, X., et al. (2015). Loss of KLF14 triggers centrosome amplification and tumorigenesis. *Nat. Commun.* **6**, 8450.
49. Li, F., Mao, G., Tong, D., Huang, J., Gu, L., Yang, W., and Li, G.-M. (2013). The Histone Mark H3K36me3 Regulates Human DNA Mismatch Repair through Its Interaction with MutS $\alpha$ . *Cell* **153**, 590–600.

## STAR★METHODS

### KEY RESOURCES TABLE

REAGENT or RESOURCE	SOURCE	IDENTIFIER
<b>Antibodies</b>		
ANTI-FLAG® antibody	Sigma-Aldrich	Cat# F7425RRID: AB_439687
Monoclonal Anti-β-Actin Antibody	Sigma-Aldrich	Cat# A5441 RRID: AB_476744
GFP Antibody (15)	Santa Cruz Biotechnology	Cat# sc-101525 RRID: AB_1563142
SIRT7 Antibody	Signalway Antibody	Cat# 32106 RRID: AB_3674124
HA tag Polyclonal Antibody	Proteintech	Cat# 51064-2-AP RRID: AB_11042321
MLH1 Recombinant Antibody	Proteintech	Cat# 84208-2-RR RRID: AB_3671764
PMS2 Monoclonal antibody	Proteintech	Cat# 66075-1-Ig RRID: AB_11182595
GST Tag Monoclonal Antibody	Proteintech	Cat# 66001-2-Ig RRID: AB_2881488
6*His, His-tag Polyclonal Antibody	Proteintech	Cat# 10001-0-AP RRID: AB_11232228
Anti-MSH2 Antibody [3A2B8C]	Abcam	Cat# ab52266 RRID: AB_2144800
Anti-MSH6 Antibody [EPR3945]	Abcam	Cat# ab92471 RRID: AB_2144959
Phospho-(Ser/Thr) Phe Antibody	CST	Cat# 9631 RRID: AB_330308
Acetylated-Lysine Antibody	CST	Cat# 9441 RRID: AB_331805
Phospho-(Ser/Thr) ATM/ATR Substrate Antibody	CST	Cat# 2851 RRID: AB_330318
<b>Bacterial and virus strains</b>		
Trans1-T1 Phage Resistant Chemically Competent Cell	TransGen Biotech	CD501-2
Transetta(DE3) Chemically Competent Cell	TransGen Biotech	CD801-02
BL21(DE3) Chemically Competent Cell	TransGen Biotech	CD601-02
<b>Biological samples</b>		
Human Cervical Cancer Tissue Chip	Shanghai Superbiotek Pharmaceutical Technology Co., Ltd	CXC481
Human Lung Cancer Tissue Chip	Shanghai Outdo Biotek Co., Ltd.	HLug-Squ150Sur-02
<b>Chemicals, peptides, and recombinant proteins</b>		
6-TG	MCE	Cat# HY-13765
6-MP	MCE	Cat# HY-13677
CPT	MCE	Cat# HY-16560
TMZ	MCE	Cat# HY-17364
MNNG	MCE	Cat# HY-128612
Etoposide	MCE	Cat# HY-13629
Mitomycin C	MCE	Cat# HY-13316
Cisplatin	MCE	Cat# HY-17394
Gemcitabine	MCE	Cat# HY-17026
MG132	Sigma-Aldrich	Cat# M7449

(Continued on next page)

**Continued**

REAGENT or RESOURCE	SOURCE	IDENTIFIER
CHX	Sigma-Aldrich	Cat# C4859
AZD6738	MCE	Cat# HY-19323
AZD1390	MCE	Cat# HY-109566
VE822	MCE	Cat# HY-13902
Caffeine	MCE	Cat# HY-103164
<b>Deposited data</b>		
Mass spectrometry data	This study	<a href="#">Table S1</a>
<b>Experimental models: Cell lines</b>		
HEK293T	ATCC	CRL-3216
HeLa	ATCC	CRM-CCL-2
H1299	ATCC	CRL-5803
HCT116	ATCC	CCL-247EMT
MDA-MB-231	ATCC	CRM-HTB-26
<b>Experimental models: Organisms/strains</b>		
BALB/c Nude	Shanghai Model Organisms	SM-0114
<b>Oligonucleotides</b>		
SIRT7-ShRNA	This Study	Not Available
F: CCGGCTTCAGAAAGGGAGAACGTT CTCGAGAACGCTTCT CCCTTTCTGAAGTTTTG		
R: AATTCAAAAACCTCAGAAAGGGAGAA GCGTTCTCGAGAAC GCTTCTCCCTTCTGAAG		
SIRT7-KO-gRNA: CGGGCCTGCCGTGTGAGG	This Study	Not Available
MSH2-ShRNA	This Study	Not Available
F: CGGCCAGTAATGGAATGAAGGTA ACTCGAGTTACCTTCATT CATTACTGGTTTTG		
R: ATTCAAAAACAGTAATGGAATGA AGGTAACTCGAGTTACCT TCATTCCTTACTGG		
<b>Software and algorithms</b>		
GraphPad Prism 10	GraphPad	<a href="https://www.graphpad.com/">https://www.graphpad.com/</a>
ImageJ	National Institutes of Health	<a href="https://imagej.net/ij/">https://imagej.net/ij/</a>
<b>Other</b>		
Anti-MSH2-K882 Acetylation Antibody	This Study	Not Available
Anti-SIRT7 Phospho-S166 Antibody	This Study	Not Available

## EXPERIMENTAL MODEL AND SUBJECT DETAILS

### Cell culture and plasmids

HeLa, H1299, HEK293T, MBA-MD-231 and HCT116 cells were maintained in DMEM with 10% (v/v) fetal bovine serum. SIRT7-knockdown plasmids were previously generated.<sup>27</sup> SIRT7 and MSH2 mutants were generated using site-directed mutagenesis. 6-TG, 6-MP, TMZ, MNNG, AZD6378, AZD1390, VE822 and caffeine obtained from Sigma. Antibodies were purchased from Sigma (FLAG, β-Actin, and Flag-M2 beads), Santa Cruz (GFP), SIRT7 (Signalway Antibody), Proteintech (GST, His, HA, MLH1, PMS2), Abcam (MSH2 and MSH6), and CST (P-Thr/Ser, Pan-Acetyl, p-ATM/ATR). A rabbit antiserum against MSH2 acetylation at K882 was raised against peptide YLEREQGEK (ac) IIQEFLS. A rabbit antiserum against SIRT7 phosphorylation at S166 was raised against peptide QHVVS (p) QNCDGLHLRS. The antiserum was purified by affinity chromatography. ShRNA used in this study are listed in the [key resources table](#).

**Animal studies**

Cells were subcutaneously injected into both flanks of male BALB/c nude mice (~ five weeks of age). Twelve days after injection, mice were treated with PBS or 6-TG (20 mg/kg) by intraperitoneal injection every five days. Tumor size was measured every five days using calipers. Animals were treated according to high ethical and scientific standards with oversight by the Animal center at Shandong University of Technology.

**METHOD DETAILS****Immunoprecipitation and western blotting**

Cell lysate preparation and western blotting were performed as previously described.<sup>27</sup> For Co-immunoprecipitation, cell lysates were immunoprecipitated with anti-Flag-M2 agarose or Protein A/G agarose plus anti-MSH2 or anti-SIRT7 antibodies for 4–6 h at 4°C. The beads were washed extensively with lysis buffer, boiled in SDS sample buffer, fractionated by SDS-PAGE, and analyzed by Western blotting using specific antibodies.

**Immunofluorescence staining**

Immunofluorescence was performed as previously described.<sup>44</sup> Briefly, cells were fixed in 4% formaldehyde, immunostained for 2 h with primary antibodies followed by a 2 h exposure to Alexa Fluor 488- or 568-conjugated secondary antibodies. Immunofluorescence was visualized using fluorescence microscopy and analyzed by ImageJ software (<https://imagej.net/ij/>).

**Cell death analyses**

Cell survival was determined by MTT assay as previously described.<sup>44</sup> In brief, the cells were incubated with MTT for 2 to 4 h, followed by the addition of 100 µL of DMSO. Then, the absorbance was measured at 450 nm using a microplate reader at the indicated time points after seeding.

**Mass spectrometry analysis**

The 293T cells maintained in normal growth medium were transfected with Flag-SIRT7 or Flag-MSH2 plasmids. Transfected cells were harvested 24 h post-transfection and lysed. Flag-SIRT7 or MSH2 were immunoprecipitated with Flag-M2 beads, eluted with Flag-peptide (Sigma), subjected to SDS-PAGE, and visualized using Coomassie Blue staining. The Flag-SIRT7 or Flag-MSH2 band was excised, destained, and digested in 50 mM ammonium bicarbonate with 12.5 ng/mL of trypsin. Peptide mixtures were analyzed online with a hybrid Q-Exactive mass spectrometer. Mass spectra were searched using the SEQUEST algorithm against a Uniprot human database. All peptide matches were initially filtered based on enzyme specificity, mass measurement error, Xcorr and Corr scores and further manually validated for peptide identification and phosphorylation site or acetylation site localization.

**MMR assay**

The MMR assay was conducted as previously described.<sup>45,46</sup> In brief, cells were plated in 12-well plates at a density of  $2 \times 10^5$  cells per well. Each well was transfected with a plasmid mixture consisting of 800 ng of pmax-vector, 100 ng of pmax-BFP, and 100 ng of pmax-mOrange (vector control) or pmax-G:G-mismatch-mOrange (MMR). After 24 h of transfection, the cells were harvested and analyzed using flow cytometry. The relative MMR capacity was calculated by dividing the percentage of mOrange-positive cells in the MMR group by the percentage of mOrange-positive cells in the vector control group. The pmax-BFP in each group served as an internal control to normalize mOrange expression.

**Mutability assay**

The mutation assay was performed as described previously.<sup>47</sup> Cells ( $5 \times 10^5$ ) were seeded in triplicate 100 mm dishes for 12 h and cultured with complete medium containing 2 µM 6-thioguanine (6-TG). The plating efficiency was determined by culturing  $5 \times 10^2$  cells in the absence of 6-TG. After 14 days, cell colonies were visualized by staining with 0.05% crystal violet. The mutation frequency was determined by dividing the number of 6-TG-resistant colonies by the total number of cells plated after being corrected for the colony-forming ability.

**Tissue microarray and IHC staining**

Human tissue microarrays of cervical cancer (CXC481, Shanghai Superbiotek Pharmaceutical Technology Co., Ltd.) and lung cancer (HLug-Squ150Sur-02, Shanghai Outdo Bioteck Co., Ltd.) were purchased. The clinical characteristics of all samples were downloaded from the Web sites of companies. Antibodies against SIRT7 and MSH2 were used for immunohistochemistry staining. The intensity of SIRT7 and MSH2 staining was quantified, scored and graded (low, 0–4 point; medium, 5–8 point; and high, 9–12 point) as described previously.<sup>48</sup> To ensure an unbiased result, data was collected in a double-blinded manner.

**Microsatellite instability assay**

Microsatellite analysis using fluorescence-labeled primers and an automated DNA sequencer has been described in detail.<sup>49</sup> Briefly, four human dinucleotide microsatellites, BAT-25, BAT-26, NR-24 and SEC-63, were amplified by polymerase chain reaction (PCR).

Forward primers were labeled with the fluorescent compound, 6-FAM (6-carboxyfluorescein). *TaKaRa Taq* (TaKaRa Co. Ltd., Tokyo, Japan) was used as a thermostable polymerase. To compare electrophoretic profiles between two samples, 6-FAM-labelled products were mixed and co-electrophoresed in the ABI310 sequencer (Applied Biosystems, Foster City, CA, USA). Data were processed using the GeneScan software (Applied Biosystems).

#### QUANTIFICATION AND STATISTICAL ANALYSES

Statistical analysis was carried out using two-tailed Student's t test, and the results are expressed as the mean  $\pm$  standard deviation (SD) of three independent experiments.  $p$  values are indicated in the Figure legends. Values of  $p < 0.05$  were considered significant. Microscopy images shown are representative of at least 5 fields from 3 independent experiments. Western Blot images are representative of 2 independent experiments. All biological and biochemical experiments were performed with appropriate internal negative Prism 10 software environment (<https://www.graphpad.com/>).